INTERNATIONAL JOURNAL FOR NUMERICAL METHODS IN ENGINEERING
Int. J. Numer. Meth. Engng 2006; **65**:147–173
Published online 7 September 2005 in Wiley InterScience (www.interscience.wiley.com). DOI: 10.1002/nme.1439

Non-linear finite element analysis of mechanical electrochemical phenomena in hydrated soft tissues based on triphasic theory

Yuan Chen[‡,§], Xian Chen[*,†,¶] and Toshiaki Hisada[‖]

School of Frontier Sciences, The University of Tokyo, 7-3-1 Hongo, Bunkyo-ku, Tokyo 113-8654, Japan

SUMMARY

The well-accepted triphasic theory for modelling the mechano-electrochemical phenomena of charged hydrated soft tissue has been limited to infinitesimal deformation problems due to the difficulty of defining a common reference configuration for the whole tissue. In this paper, an imaginary reference configuration for soft tissue under large deformation is established based on the reference configuration of a solid matrix and a Piola transformation of the relative velocities of the fluid and ionic phases. A non-linear finite element analysis formulation is proposed by applying a weighted residual method to the reformulated governing equations of triphasic theory reformulated in the imaginary reference configuration, with the displacement of the solid, fluid flows, ionic molar flows, hydrostatic pressure, and electrical potential as the unknown variables. After verifying the proposed finite-element formulation by comparing the results of a linear-confined compression problem with those obtained by the finite difference method, the numerical analysis of a three-dimensional free-swelling problem of articular cartilage with large deformation, and a strong non-linearity in the material properties is carried out to reproduce the curling behaviour of articular cartilage strips *in vitro* when submerged in solution baths of various concentrations. The results obtained by finite element analysis are in agreement with those measured experimentally. Copyright © 2005 John Wiley & Sons, Ltd.

KEY WORDS: hydrated soft tissue; triphasic theory; finite deformation; finite element analysis

1. INTRODUCTION

Hydrated soft tissue, such as articular cartilage, is composed of a relatively small number of cells (known as chondrocytes), and extracellular material which consists primarily of interstitial water

*Correspondence to: Xian Chen, School of Frontier Sciences, The University of Tokyo, 7-3-1 Hongo, Bunkyo-ku, Tokyo 113-8654, Japan.
†E-mail: xchen@sml.k.u-tokyo.ac.jp
‡E-mail: chenyuan@sml.k.u-tokyo.ac.jp
§Postdoctoral Fellow.
¶Associate Professor.
‖Professor.

Contract/grant sponsor: The Japan Society for the Promotion of Science through a Grant-in-Aid for Scientific Research; contract/grant number: (C) 14550067
Contract/grant sponsor: Core Research for Evolutional Science and Technology of the Japan Science and Technology

Received 13 September 2004
Revised 30 March 2005
Accepted 24 June 2005

(70–85% of weight) and complex collagen-proteoglycans solid networks termed extracellular matrix (ECM). The proteoglycan aggregates are negatively charged by the attached sulphated glycosaminoglycans charges at physiologic pH, and the charge state is characterized by a fixed charge density (FCD). Also, the electrolyte, sodium and chloride are the dominant ions dissolved in the interstitial water [1]. Such a multiphasic nature of the tissue, especially the existence of ions and fixed charges, induces mechanical electrochemical coupling phenomena such as swelling [2–6], streaming potential [7] and electroosmosis [7].

To investigate mechanical electrochemical coupling phenomena in soft tissues, two main types of theoretical models have been proposed based on poroelastic consolidation theory [8] and mixture theory [9]. In the latter, the well-accepted triphasic mechano-electrochemical theory developed by Lai *et al.* [10] has been widely applied to the study of soft tissue, such as articular cartilage and intervertebral discs (e.g. References [11–13]). In this theory, the hydrated soft tissue is regarded as a mixture composed of a negatively charged solid matrix as the incompressible solid phase, interstitial water as the incompressible fluid phase, and the ionic phase including both cations and anions. Since all phases are assumed to occupy the same infinitesimal space simultaneously but with their own reference configurations, the common reference configuration of the whole of the tissue is hard to define in the case of large deformation due to the movements of the fluid and ionic phases. Therefore, applications of this theory have been limited to infinitesimal deformation problems [10]. For large deformations, Huyghe *et al.* [14] have developed a quadriphasic mixture theory (counting the cation and anion phases as separate) starting from the derivation of a 'Lagrangian form' of the entropy inequality with respect to the initial solid state. However, physical explanations of the introduced 'Lagrangian form' of the variables regarding the fluid and ionic phases, such as the relative velocities, have yet to be discussed.

Because of the complexities of these theoretical models describing mechanical electrochemical phenomena, analytical solutions can only be obtained for quite simplified problems, such as linear-confined problems [15]. Therefore, an appropriate choice is the use of numerical procedures for applications such as finite element analysis (FEA). In the category of mixture theory, Sun *et al.* [16] first developed a linear finite element formulation for one-dimensional infinitesimal problems based on triphasic theory. On the other hand, Frijns *et al.* [17] and Loon *et al.* [18] proposed finite element formulations based on the quadriphasic theory developed by Huyghe *et al.* [14] for one- and three-dimensional problems of intervertebral discs and hydrogel, respectively. In these formulations, instead of the relative velocities of the fluid and ions to solid, the chemical potential of the fluid and the electrochemical potentials of the ions have been taken as the unknown variables to reduce the degrees of freedom. However, the derivatives of the chemical and electrochemical potentials with respect to the spatial co-ordination included in the resulting weak forms limit the selection of interpolation functions for these potentials to linear or higher order. Also, the accuracy of the relative velocities of the fluid and ionic phases may be reduced since they are calculated from the gradients of the chemical and electrochemical potentials. For example, the velocities will become constant within an element if linear interpolation functions for chemical and electrochemical potentials are selected. Furthermore, in these studies, the numerical examples were limited to traditional confined and unconfined problems, and the mechanical electrochemical behaviours of soft tissue undergoing large deformations were not well investigated.

In this research, to extend the application of triphasic theory to finite deformation problems, an imaginary common reference configuration for the whole of the tissue under large

deformation is established for the purpose of applying the approaches used for single continua, while preserving the kinematics of the fluid and ionic phases by applying a Piola transformation to the relative velocities. Then, the governing equations of triphasic theory are reformulated based on mapping from the current configuration to an imaginary one. Moreover, a non-linear finite element formulation is obtained by applying the weighted residual method to the reformulated governing equations. In contrast with previous studies [17, 18], the relative velocities of the fluid and ionic phases are chosen as the unknown variables along with the displacement of the solid, the hydrostatic pressure, and the electrical potential. This way, interelement discontinuous interpolation functions are allowed for the hydrostatic pressure and the electrical potential. The relative velocities, which are important in clinical and biological applications, can be obtained directly to improve the accuracy. To assess the validity and effectiveness of the proposed approach, a couple of numerical examples are analysed for isotropic materials. After verifying the proposed finite element formulation using a linear-confined compression problem, the effects of the non-linearities of the porosity and the FCD on the behaviours of soft tissue are discussed. Furthermore, a three-dimensional free-swelling problem of articular cartilage with large deformation is simulated by taking into account the deformation-dependent permeability and non-uniform distributions of FCD and solidity. The numerical results reproduce the curling behaviours of cartilage strips *in vitro* when submerged in solution baths of various concentrations. The swelling parameters [19], such as the swelling-reduced stretching and areal changes obtained by FEA are in agreement with those measured by experiment. To the author's knowledge, numerical simulations of the coupling behaviours of soft tissue undergoing large deformations have yet to be reported upon in the literature. It is worth mentioning that, although the numerical simulations are carried out for isotropic materials, the formulation in this work is performed without the assumption of isotropy and can be applied to anisotropic materials if the anisotropic constitutive relation for the solid phase and anisotropic permeability and diffusion coefficient tensors are introduced.

2. GOVERNING EQUATIONS OF THE TRIPHASIC THEORY AND REFORMULAION FOR LARGE DEFORMATION PROBLEMS

2.1. Governing equations

In triphasic theory [10], all phases (constituents) of the soft tissue are assumed to occupy the same infinitesimal space simultaneously. Each constituent is characterized by the volume fraction defined as

$$\phi^\alpha = \frac{\rho^\alpha}{\rho_{\mathrm{T}}^\alpha} \quad (\alpha = \mathrm{s}, \mathrm{w}, +, -) \tag{1}$$

where superscripts s, w, + and − denote the solid, fluid, cation and anion constituents, respectively; ρ^α denotes the apparent density defined as the mass of the α constituent per unit tissue volume; and ρ_{T}^α is the real density (true density) of the α constituent. For hydrated soft tissue, the saturation condition satisfies the following condition

$$\sum_{\alpha=\mathrm{s}, \mathrm{w}, +, -} \phi^\alpha = 1 \tag{2}$$

The continuity equation is given by

$$\frac{\partial \rho^{\alpha}}{\partial t} + \nabla \cdot (\rho^{\alpha} \mathbf{v}^{\alpha}) = 0 \quad (\alpha = \mathrm{s}, \mathrm{w}, +, -) \tag{3}$$

where $\partial/\partial t$ denotes the spatial time derivative and $\mathbf{v}^{\alpha}$ is the velocity of each constituent. Assuming intrinsic incompressibility for each constituent and neglecting the fairly small ionic volumes reduces the incompressible constraint condition for the tissue to

$$\nabla \cdot (\phi^{\mathrm{s}} \mathbf{v}^{\mathrm{s}} + \phi^{\mathrm{w}} \mathbf{v}^{\mathrm{w}}) = 0 \tag{4}$$

where the volume fractions ϕ^{s} and ϕ^{w} are called the solidity and porosity, respectively.

In triphasic theory, the velocities of the fluid and ionic phases relative to the solid phase are defined as $\mathbf{w} = \phi^{\mathrm{w}}(\mathbf{v}^{\mathrm{w}} - \mathbf{v}^{\mathrm{s}})$ and $\mathbf{j}^{\alpha} = \tilde{c}^{\alpha}(\mathbf{v}^{\alpha} - \mathbf{v}^{\mathrm{s}})$ $(\alpha = +, -)$ in the sense of the fluid and ionic molar fluxes. By assuming that the cation–cation, anion–anion, and ion–solid frictions are negligible compared to the solid– and ion–fluid frictions [11], the quasi-static momentum equations of the tissue, fluid and ionic phases are given by

$$\nabla \cdot \boldsymbol{\sigma} = \mathbf{0} \tag{5}$$

$$\rho_{\mathrm{T}}^{\mathrm{w}} \nabla \mu^{\mathrm{w}} = -\boldsymbol{\kappa}^{-1} \cdot \mathbf{w} - \frac{c^{+} RT}{\phi^{\mathrm{w}}} \mathbf{d}^{+^{-1}} \cdot \mathbf{w} - \frac{c^{-} RT}{\phi^{\mathrm{w}}} \mathbf{d}^{-^{-1}} \cdot \mathbf{w} + \frac{RT}{\phi^{\mathrm{w}}} \mathbf{d}^{+^{-1}} \cdot \mathbf{j}^{+} + \frac{RT}{\phi^{\mathrm{w}}} \mathbf{d}^{-^{-1}} \cdot \mathbf{j}^{-} \tag{6}$$

$$M^{+} \nabla \tilde{\mu}^{+} = \frac{RT}{\phi^{\mathrm{w}}} \mathbf{d}^{+^{-1}} \cdot \mathbf{w} - \frac{RT}{\tilde{c}^{+}} \mathbf{d}^{+^{-1}} \cdot \mathbf{j}^{+} \tag{7}$$

$$M^{-} \nabla \tilde{\mu}^{-} = \frac{RT}{\phi^{\mathrm{w}}} \mathbf{d}^{-^{-1}} \cdot \mathbf{w} - \frac{RT}{\tilde{c}^{-}} \mathbf{d}^{-^{-1}} \cdot \mathbf{j}^{-} \tag{8}$$

where $\boldsymbol{\sigma}$ is the total Cauchy stress tensor of the tissue, μ^{w}, $\tilde{\mu}^{+}$ and $\tilde{\mu}^{-}$ are the chemical potential of the fluid and the electrochemical potentials of the cation and anion per unit mass, respectively. $\boldsymbol{\kappa}$ and $\mathbf{d}^{\alpha}$ $(\alpha = +, -)$ represent the permeability and ionic diffusion coefficients, R and T denote the universal gas constant and absolute temperature, respectively, c^{α} $(\alpha = +, -)$ is the ionic molar concentration defined as the mole of ions per unit volume of interstitial water, M^{α} $(\alpha = +, -)$ denotes the ionic molecular weight related to the apparent densities of ions as $\rho^{\alpha} = c^{\alpha} \phi^{\mathrm{w}} M^{\alpha}$, while $\tilde{c}^{\alpha}$ $(\alpha = +, -)$ is the ionic molar concentration defined as a mole of α constituent per unit volume of tissue and related to c^{α} by $\tilde{c}^{\alpha} = c^{\alpha} \phi^{\mathrm{w}}$. Furthermore, under the assumption that the viscosities of both the solid and fluid phases can be neglected, the total Cauchy stress for the whole tissue, the chemical and electrochemical potentials for the fluid and the univalent ions are, respectively,

$$\boldsymbol{\sigma} = -p\mathbf{I} + \boldsymbol{\sigma}^{\mathrm{e}} \tag{9}$$

$$\mu^{\mathrm{w}} = \mu_0^{\mathrm{w}} + \frac{p}{\rho_{\mathrm{T}}^{\mathrm{w}}} - \frac{RT}{\rho_{\mathrm{T}}^{\mathrm{w}}} \Phi(c^{+} + c^{-}) \tag{10}$$

$$\tilde{\mu}^{+} = \mu_0^{+} + \frac{RT}{M^{+}} \ln(\gamma^{+} c^{+}) + \left(\frac{\eta}{M^{+}}\right) \tag{11}$$

$$\tilde{\mu}^- = \mu_0^- + \frac{RT}{M^-}\ln(\gamma^- c^-) - \left(\frac{\eta}{M^-}\right) \tag{12}$$

where p is the hydrostatic pressure, $\mathbf{I}$ denotes the identity tensor, $\boldsymbol{\sigma}^e$ is the part of the stress produced by the elastic deformation of the solid matrix, μ_0^α ($\alpha = w, +, -$) is the reference chemical potential for the α constituent, Φ is the osmotic coefficient assumed to be the same for cations and anions, $\gamma^\pm$ are the activity coefficients of the cation and anion, and η is the product of the Faraday constant and the electric potential.

Substituting the definition of the relative fluid velocity $\mathbf{w}$ into Equation (4) yields the incompressible constraint condition in the form

$$\nabla \cdot (\mathbf{v}^s + \mathbf{w}) = 0 \tag{13}$$

The electroneutral requirement for the tissue leads the constraint of electroneutrality for univalent solutes to

$$\tilde{c}^+ - \tilde{c}^- - \tilde{c}^F = 0 \tag{14}$$

where $\tilde{c}^F$ is the negative fixed-charge density in the equivalent mole per unit tissue volume with the relationship to that defined in the unit volume of interstitial water by $\tilde{c}^F = c^F \phi^w$.

Accordingly, the boundary conditions are given by

$$\boldsymbol{\sigma} \cdot \mathbf{n} = \mathbf{f}^* \quad \text{on } \Gamma_t \tag{15}$$

$$\mu^w = \mu^{w*} \quad \text{on } \Gamma_w \tag{16}$$

$$\tilde{\mu}^+ = \tilde{\mu}^{+*} \quad \text{on } \Gamma_+ \tag{17}$$

$$\tilde{\mu}^- = \tilde{\mu}^{-*} \quad \text{on } \Gamma_- \tag{18}$$

where the superscript * indicates the prescribed boundary values, $\mathbf{n}$ is the unit outward normal vector of the surface, and $\mathbf{f}^*$ is the traction applied on the boundary Γ_t. Correspondingly, the fluid chemical potential and ionic electrochemical potentials are prescribed on the boundaries Γ_w, Γ_+, and Γ_-, respectively. Specifying the boundary conditions on the whole of the boundary Γ of the tissue requires descriptions of the solid displacement $\mathbf{u}^s$ (or velocity $\mathbf{v}^s$) on Γ_{us}, the relative velocity of the fluid $\mathbf{w}$ on Γ_{jw}, the relative velocity of the cation $\mathbf{j}^+$ on Γ_{j+} and that of the anion $\mathbf{j}^-$ on Γ_{j-}. The complementary portions of Γ have the relationships

$$\Gamma = \Gamma_t \cup \Gamma_{us} = \Gamma_w \cup \Gamma_{jw} = \Gamma_+ \cup \Gamma_{j+} = \Gamma_- \cup \Gamma_{j-} \tag{19}$$

$$\Gamma_t \cap \Gamma_{us} = \Gamma_w \cap \Gamma_{jw} = \Gamma_+ \cap \Gamma_{j+} = \Gamma_- \cap \Gamma_{j-} = \varnothing \tag{20}$$

The boundary conditions with respect to $\mathbf{w}$, $\mathbf{j}^+$ and $\mathbf{j}^-$ can be determined from the balance of the mass on the boundaries and may be discontinuous between the inside and outside of the tissue [20].

2.2. *Reformulation for large deformation problems*

In mixture-based triphasic theory, the assumption that all constituents occupy the same spatial location simultaneously, implies that the mapping for each constituent leads to a different

reference configuration due to the relative movements with respect to each other. Thus, a common reference configuration for the whole tissue is hard to define directly for utilizing the approaches in single-phase continuum mechanics for large deformations. By utilizing the reference configuration of the solid phase, while keeping the velocity of the fluid phase defined in the current configuration, a finite element formulation for soft tissue under large deformation has been proposed by Suh *et al.* [21] based on biphasic theory [22]. In biphasic theory, the tissue is treated as a mixture of solid and fluid while the ionic effects are excluded. In the present work, consistent with the mixture description, each constituent should be dealt with equivalently. Although in principle, mapping of each constituent exists between its own reference and current configurations, considering that the deformation of the solid matrix coincides with that of the tissue, and that the constitutive models of the solid matrix are usually provided in Lagrangian form by assuming that the solid matrix of soft tissues is elastic material, it is natural to introduce a mapping for the tissue by tracing the deformation of the solid matrix. Meanwhile, the relative velocities of the non-solid phases can be transformed to the reference configuration of the solid phase via a Piola transformation. In this way, an imaginary reference configuration of the tissue can be defined in order to evaluate the physical quantities and reformulate the governing equations as in the case of a single-phase continuum. It should be mentioned that a Piola transformation for the relative velocities of non-solid phases has been introduced in the context of poroelastic consolidation theory [23], whereas in the present work, a Piola transformation is applied to establish an imaginary reference configuration in the framework of mixture theory.

In mixture theory [9], being regarded as a continuum, each constituent is assigned a fixed but otherwise arbitrary reference configuration and its motion is described as

$$\mathbf{x} = \xi^{\alpha}(\mathbf{X}^{\alpha}, t) \quad (\alpha = \mathrm{s}, \mathrm{w}, +, -) \tag{21}$$

where $\mathbf{X}^{\alpha}$ denotes the initial position of the particle of α constituent and ξ^{α} is a deformation function. Correspondingly, the deformation gradient tensor of the α constituent can be defined as $\mathbf{F}^{\alpha} \equiv \mathrm{d}\mathbf{x}/\mathrm{d}\mathbf{X}^{\alpha}$, and thus, $J^{\alpha} \equiv \det \mathbf{F}^{\alpha}$ gives its volume change. In the present research, however, by applying a Piola transformation associated with the deformation gradient of the solid matrix $\mathbf{F}^{\mathrm{s}}$ to the relative velocities of the fluid and ionic phases, i.e.

$$\mathbf{W}^{\mathrm{s}} = J^{\mathrm{s}}\mathbf{F}^{\mathrm{s}^{-1}} \cdot \mathbf{w} \tag{22}$$

$$\mathbf{J}^{\alpha\mathrm{s}} = J^{\mathrm{s}}\mathbf{F}^{\mathrm{s}^{-1}} \cdot \mathbf{j}^{\alpha} \quad (\alpha = +, -) \tag{23}$$

two important properties are obtained as

$$\nabla_0^{\mathrm{s}} \cdot \mathbf{W}^{\mathrm{s}}\,\mathrm{d}V^{\mathrm{s}} = \nabla \cdot \mathbf{w}\,\mathrm{d}v, \quad \nabla_0^{\mathrm{s}} \cdot \mathbf{J}^{\alpha\mathrm{s}}\,\mathrm{d}V^{\mathrm{s}} = \nabla \cdot \mathbf{j}^{\alpha\mathrm{s}}\,\mathrm{d}v \ (\alpha = +, -) \tag{24}$$

$$\mathbf{W}^{\mathrm{s}} \cdot \mathbf{N}^{\mathrm{s}}\,\mathrm{d}S^{\mathrm{s}} = \mathbf{w} \cdot \mathbf{n}\,\mathrm{d}s, \quad \mathbf{J}^{\alpha\mathrm{s}} \cdot \mathbf{N}^{\mathrm{s}}\,\mathrm{d}S^{\mathrm{s}} = \mathbf{j}^{\alpha} \cdot \mathbf{n}\,\mathrm{d}s \ (\alpha = +, -) \tag{25}$$

where ∇, $\mathrm{d}v$, $\mathrm{d}s$ and $\mathbf{n}$ denote the spatial differential operator, infinitesimal volume element, infinitesimal surface element and unit outward normal vector of the surface, respectively, which are all defined in the current configuration; their counterparts in the imaginary reference

configuration of the solid matrix are denoted as ∇_0^s, dV^s, dS^s, and $\mathbf{N}^s$, respectively. Equations (24) and (25) indicate that the Piola transformation preserves the kinematics of the fluid and ions, in the sense of representing the dilatation and flow by divergence and flux. Thus, if defining a mapping for the tissue by means of mapping the solid matrix and a Piola transformation of the relative velocities of the non-solid phases, an imaginary reference configuration can now be established by including the reference configuration of the solid matrix and the Piola transformed relative fluid and ionic velocities. Figure 1 gives a demonstration of the imaginary reference configuration where a cation is taken as an example. Piola transformations of the relative velocities can be regarded as images of the relative movements of fluid and ions, which are measured by an observer convected with the deformation of the solid phase. For simplicity, the superscript s will be omitted hereinafter.

After introducing the imaginary reference configuration, similar to the approach applied to the single-phase continuum, the governing equations of triphasic theory are reformed by evaluating variables of the tissue and each constituent in the imaginary reference configuration. Regarding the total Cauchy stress of the tissue, its Piola transformation leads to the first Piola–Kirchhoff stress

$$\mathbf{\Pi} = J\mathbf{F}^{-1} \cdot \boldsymbol{\sigma} \tag{26}$$

which is a nominal measurement with respect to the imaginary reference configuration. According to Equation (9), the second Piola–Kirchhoff stress of the tissue is expressed by

$$\mathbf{S} = \mathbf{\Pi} \cdot \mathbf{F}^{-\mathrm{T}} = J\mathbf{F}^{-1} \cdot \boldsymbol{\sigma} \cdot \mathbf{F}^{-\mathrm{T}} = \mathbf{S}^{\mathrm{E}} - pJ\mathbf{C}^{-1} \tag{27}$$

where $\mathbf{C}$ is right Cauchy–Green deformation tensor, $\mathbf{S}^{\mathrm{E}}$ denotes the part of second Piola–Kirchhoff stress contributed by the elastic deformation of the solid phase. For the hyperelastic solid matrix, $\mathbf{S}^{\mathrm{E}}$ can be determined from the Helmholtz free energy per unit volume of solid

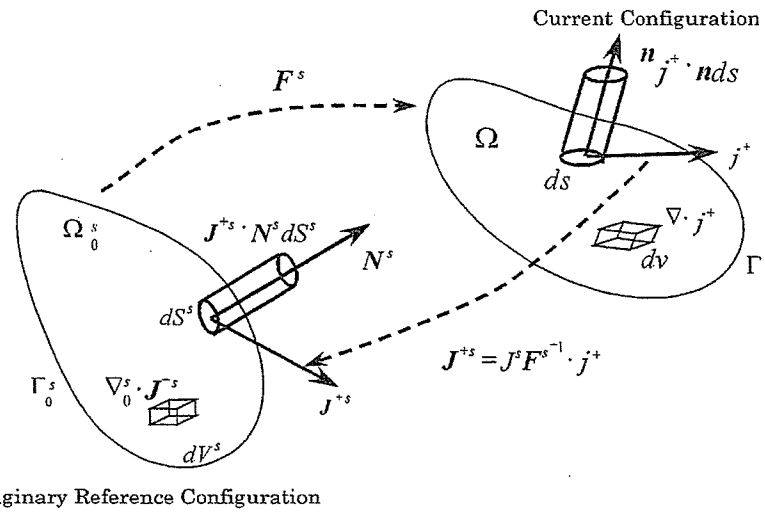

Figure 1. Demonstration of the reference configuration and Piola transformation (including the solid and cation as an example).

phase U,

$$\mathbf{S}^{\mathrm{E}} = \frac{\partial U}{\partial \mathbf{E}} \tag{28}$$

where $\mathbf{E}$ is the Green–Lagrange strain tensor.

By means of the imaginary reference configuration, the governing equations of triphasic theory can now be reformulated as follows. Substituting Equations (22), (23), (26) and (27) into Equations (5)–(8) leads to the momentum equations in the imaginary reference configuration as

$$\nabla_0 \cdot \mathbf{\Pi} = \mathbf{0} \quad \text{or} \quad \nabla_0 \cdot (\mathbf{S} \cdot \mathbf{F}^{\mathrm{T}}) = \mathbf{0} \tag{29}$$

$$-\rho_{\mathrm{T}}^{\mathrm{w}} \nabla_0 \mu^{\mathrm{w}} - \mathbf{K}^{-1} \cdot \mathbf{W} + \frac{RT}{\phi^{\mathrm{w}}} \mathbf{D}^{+^{-1}} \cdot (\mathbf{J}^{+} - c^{+}\mathbf{W}) + \frac{RT}{\phi^{\mathrm{w}}} \mathbf{D}^{-^{-1}} \cdot (\mathbf{J}^{-} - c^{-}\mathbf{W}) = \mathbf{0} \tag{30}$$

$$-M^{+} \nabla_0 \tilde{\mu}^{+} - \frac{RT}{\tilde{c}^{+}} \mathbf{D}^{+^{-1}} \cdot (\mathbf{J}^{+} - c^{+}\mathbf{W}) = \mathbf{0} \tag{31}$$

$$-M^{-} \nabla_0 \tilde{\mu}^{-} - \frac{RT}{\tilde{c}^{-}} \mathbf{D}^{-^{-1}} \cdot (\mathbf{J}^{-} - c^{-}\mathbf{W}) = \mathbf{0} \tag{32}$$

where the relationship $\nabla_0 b = \mathbf{F}^{\mathrm{T}} \cdot \nabla b$ for an arbitrary scalar b was used to obtain the above equations. The permeability and ionic diffusion coefficients in the imaginary reference configuration become

$$\mathbf{K} = J\mathbf{F}^{-1} \cdot \boldsymbol{\kappa} \cdot \mathbf{F}^{-\mathrm{T}} \tag{33}$$

$$\mathbf{D}^{\alpha} = J\mathbf{F}^{-1} \cdot \mathbf{d}^{\alpha} \cdot \mathbf{F}^{-\mathrm{T}} \quad (\alpha = +, -) \tag{34}$$

Considering that the constitutive relationship of the solid matrix is usually given as a function of the total strain, and also, the initial ionic concentrations and FCD are in practice usually known, it is convenient to formulate the incompressible and electroneutral constraint conditions based on the accumulated forms of fluid flux and ionic molar fluxes as follows.

The volumetric fluid flux and ionic molar fluxes from the infinitesimal surface element are defined as

$$\mathrm{d}\dot{V} = \mathbf{W} \cdot \mathbf{N}\,\mathrm{d}S \tag{35}$$

$$\mathrm{d}\dot{I}^{\alpha} = \mathbf{J}^{\alpha} \cdot \mathbf{N}\,\mathrm{d}S \quad (\alpha = +, -) \tag{36}$$

The corresponding outward vectors of the accumulated fluid flow and ionic molar flows per unit area in a certain period of time, denoted by $\mathbf{Q}$ and $\mathbf{Q}^{\alpha}$, are introduced via

$$\mathrm{d}V = \mathbf{Q} \cdot \mathbf{N}\,\mathrm{d}S \tag{37}$$

$$\mathrm{d}I^{\alpha} = \mathbf{Q}^{\alpha} \cdot \mathbf{N}\,\mathrm{d}S \quad (\alpha = +, -) \tag{38}$$

Therefore, the fluxes and flows are related by

$$\dot{\mathbf{Q}} = \mathbf{W} \tag{39}$$

$$\dot{\mathbf{Q}}^{\alpha} = \mathbf{J}^{\alpha} \tag{40}$$

Thus, substituting Equations (22), (39) and identity $\dot{J} = J\nabla\cdot\mathbf{v}^{s}$ into the incompressible constraint condition (13) leads to the form in reference configuration as

$$\dot{J} + \nabla_0 \cdot \dot{\mathbf{Q}} = 0 \tag{41}$$

Furthermore, integrating Equation (41) with respect to time and noting $J(t=0)=1$, $\mathbf{Q}(t=0)=\mathbf{0}$, the incompressible constraint condition is reformulated as

$$J - 1 + \nabla_0 \cdot \mathbf{Q} = 0 \tag{42}$$

Regarding the electroneutral constraint condition, Equation (14) is transformed to the imaginary reference configuration as

$$\tilde{C}^{+} - \tilde{C}^{-} - \tilde{C}^{F} = 0 \tag{43}$$

where $\tilde{C}^{\alpha} = J\tilde{c}^{\alpha}$ $(\alpha = +, -)$ and $\tilde{C}^{F} = J\tilde{c}^{F}$ are the ionic concentration and FCD per unit volume of tissue in the imaginary reference configuration, respectively. The accumulated ionic molar outflow per unit volume of the tissue can be obtained as $\nabla_0 \cdot \mathbf{Q}^{\alpha}$ by applying the divergence theorem to Equation (38). Then, from the assumption that there is no chemical reaction, the following relationship holds

$$\tilde{C}^{\alpha} = \tilde{C}_0^{\alpha} - \nabla_0 \cdot \mathbf{Q}^{\alpha} \quad (\alpha = +, -) \tag{44}$$

where $\tilde{C}_0^{\alpha}$ denotes the initial ionic molar concentration in the imaginary reference configuration. Assuming that the fixed charges are maintained during the deformation, i.e. $\tilde{C}^{F} = \tilde{C}_0^{F}$, and considering that the initial electroneutral constraint $\tilde{C}_0^{+} - \tilde{C}_0^{-} - \tilde{C}_0^{F} = 0$ holds, the electroneutral constraint condition is reformulated in the imaginary reference configuration to be

$$-\nabla_0 \cdot \mathbf{Q}^{+} + \nabla_0 \cdot \mathbf{Q}^{-} = 0 \tag{45}$$

The merit of the above reformulations is recognized as follows. By comparing Equations (6)–(8) with (30)–(32) and (13) with (42), it is found that different differential operators appear in these two sets of equations. In Equations (6)–(8), the differential operators with respect to the spatial frame of the current configuration should be transformed if the reference configuration of the solid matrix is chosen. This manipulation will induce additional terms associate with the determinant and inverse of the deformation gradient tensor of the solid matrix like in the formulation of Suh *et al.* [21] for biphasic theory, and thus, considerably increase the complexity of the formulation. On the other hand, by introducing the relative velocities of the non-solid phases described in the reference configuration of the solid matrix and Piola's transformation, the differential operators in Equations (30)–(32) and (42) can be defined with respect to the spatial frame of the reference configuration, and thus can be directly applied to the evaluation of the variational statements in the reference configuration of the solid matrix in the finite element procedure to ensure matrix sparsity.

Additionally, the boundary conditions in the imaginary reference configuration are given by

$$\mathbf{\Pi}\cdot\mathbf{N}=\mathbf{t}^* \quad \text{or} \quad \mathbf{S}\cdot\mathbf{F}^{\mathrm{T}}\cdot\mathbf{N}=\mathbf{t}^* \quad \text{on } \Gamma_{t0} \tag{46}$$

$$\mu^{\mathrm{w}}=\mu^{\mathrm{w}^*} \quad \text{on } \Gamma_{\mathrm{w}0} \tag{47}$$

$$\tilde{\mu}^{+}=\tilde{\mu}^{+^*} \quad \text{on } \Gamma_{+0} \tag{48}$$

$$\tilde{\mu}^{-}=\tilde{\mu}^{-^*} \quad \text{on } \Gamma_{-0} \tag{49}$$

where $\mathbf{t}^*$ is the prescribed nominal traction. Boundaries Γ_{t0}, $\Gamma_{\mathrm{w}0}$, Γ_{+0} and Γ_{-0} (also Γ_{us0}, $\Gamma_{j\mathrm{w}0}$, Γ_{j+0} and Γ_{j-0}) in the imaginary reference configuration are counterparts of those in the current configuration.

3. FORMULATION OF NON-LINEAR FINITE ELEMENT ANALYSIS

Based on the reformulated governing equations in the last section, finite element formulation is carried out by taking the relative velocities of the fluid and ionic phases as unknown variables along with the displacement of the solid, the hydrostatic pressure, and the electrical potential. In this way, the interelement discontinuous interpolation functions can be used for the hydrostatic pressure and electrical potential, and also, the relative velocities of the fluid and ionic phases are obtained directly to improve accuracy.

Let Ω^{s}, Ω^{w}, Ω^{+}, Ω^{-}, Ω^{p} and Ω^{η} be spaces of arbitrary admissible weighting functions for the solid displacement, fluid flow, cation molar flow, anion molar flow, hydrostatic pressure and electrical potential, respectively. Applying the weighted residual method to the momentum equations (29)–(32), constraint conditions (42) and (45), and boundary conditions (46) to (49) gives rise to

$$\begin{aligned}
&\int_{\Omega_0}\delta\chi^{\mathrm{s}}\cdot\nabla_0\cdot(\mathbf{S}\cdot\mathbf{F}^{\mathrm{T}})\,\mathrm{d}V+\int_{\Gamma_{t0}}\delta\chi^{\mathrm{s}}\cdot(\mathbf{t}^*-\mathbf{S}\cdot\mathbf{F}^{\mathrm{T}}\cdot\mathbf{N})\,\mathrm{d}S\\
&+\int_{\Omega_0}\delta\chi^{\mathrm{w}}\cdot\left[\nabla_0(p-\pi)+\mathbf{K}^{-1}\cdot\mathbf{W}-\frac{RT}{\phi^{\mathrm{w}}}\mathbf{D}^{+^{-1}}\cdot(\mathbf{J}^{+}-c^{+}\mathbf{W})-\frac{RT}{\phi^{\mathrm{w}}}\mathbf{D}^{-^{-1}}\cdot(\mathbf{J}^{-}-c^{-}\mathbf{W})\right]\mathrm{d}V\\
&+\int_{\Gamma_{\mathrm{w}0}}\delta\chi^{\mathrm{w}}[(p^*-\pi^*)-(p-\pi)]\cdot\mathbf{N}\,\mathrm{d}S\\
&+\int_{\Omega_0}\delta\chi^{+}\cdot\left[\nabla_0(M^{+}\mu^{+}+\eta)+\frac{RT}{\tilde{c}^{+}}\mathbf{D}^{+^{-1}}\cdot(\mathbf{J}^{+}-c^{+}\mathbf{W})\right]\mathrm{d}V\\
&+\int_{\Gamma_{+0}}\delta\chi^{+}[(M^{+}\mu^{+^*}+\eta^*)-(M^{+}\mu^{+}+\eta)]\cdot\mathbf{N}\,\mathrm{d}S
\end{aligned}$$

$$+\int_{\Omega_0}\delta\chi^- \cdot [\nabla_0(M^-\mu^- - \eta) + \frac{RT}{\tilde{c}^-}\mathbf{D}^{-^{-1}}\cdot(\mathbf{J}^- - c^-\mathbf{W})]\,\mathrm{d}V$$

$$+\int_{\Gamma_{-0}}\delta\chi^-[(M^-\mu^{-^*} - \eta^*) - (M^-\mu^- - \eta)]\cdot\mathbf{N}\,\mathrm{d}S$$

$$+\int_{\Omega_0}\delta\chi^p[J - 1 + \nabla_0\cdot\mathbf{Q}]\,\mathrm{d}V + \int_{\Omega_0}\delta\chi^\eta[-\nabla_0\cdot\mathbf{Q}^+ + \nabla_0\cdot\mathbf{Q}^-]\,\mathrm{d}V = 0 \tag{50}$$

where $\delta\chi^s \in \Omega^s$, $\delta\chi^w \in \Omega^w$, $\delta\chi^+ \in \Omega^+$, $\delta\chi^- \in \Omega^-$, $\delta\chi^p \in \Omega^p$ and $\delta\chi^\eta \in \Omega^\eta$ are weighting functions; $\pi = RT\Phi(c^+ + c^-)$ and $\mu^\alpha = \mu_0^\alpha + (RT/M^\alpha)\ln(\gamma^\alpha c^\alpha)$ $(\alpha = +, -)$ are osmotic pressure and the ionic chemical potential, respectively. Also, to obtain Equation (50), Equations (10)–(12) were used.

Applying the divergence theorem to Equation (50) yields the weak form of the problem:

$$\int_{\Omega_0}(\mathbf{S}^E - pJ\mathbf{C}^{-1}) : \nabla_0 \otimes \delta\chi^s\,\mathrm{d}V$$

$$+\int_{\Omega_0}\left((p-\pi)\nabla_0\cdot\delta\chi^w - \delta\chi^w\left[\mathbf{K}^{-1}\cdot\mathbf{W} - \frac{RT}{\phi^w}\mathbf{D}^{+^{-1}}\cdot(\mathbf{J}^+ - c^+\mathbf{W}) - v\frac{RT}{\phi^w}\mathbf{D}^{-^{-1}}\cdot(\mathbf{J}^- - c^-\mathbf{W})\right]\right)\mathrm{d}V$$

$$+\int_{\Omega_0}\left((M^+\mu^+ + \eta)\nabla_0\cdot\delta\chi^+ - \delta\chi^+\left[\frac{RT}{\tilde{c}^+}\mathbf{D}^{+^{-1}}\cdot(\mathbf{J}^+ - c^+\mathbf{W})\right]\right)\mathrm{d}V$$

$$+\int_{\Omega_0}\left((M^-\mu^- - \eta)\nabla_0\cdot\delta\chi^- - \delta\chi^-\left[\frac{RT}{\tilde{c}^-}\mathbf{D}^{-^{-1}}\cdot(\mathbf{J}^- - c^-\mathbf{W})\right]\right)\mathrm{d}V$$

$$+\int_{\Omega_0}\delta\chi^p[J - 1 + \nabla_0\cdot\mathbf{Q}]\,\mathrm{d}V + \int_{\Omega_0}\delta\chi^\eta[-\nabla_0\cdot\mathbf{Q}^+ + \nabla_0\cdot\mathbf{Q}^-]\,\mathrm{d}V$$

$$-\int_{\Gamma_0}\delta\chi^s\cdot\mathbf{t}^*\,\mathrm{d}S - \int_{\Gamma_{w0}}\delta\chi^w(p^* - \pi^*)\cdot\mathbf{N}\,\mathrm{d}S$$

$$-\int_{\Gamma_{+0}}\delta\chi^+(M^+\mu^{+^*} + \eta^*)\cdot\mathbf{N}\,\mathrm{d}S - \int_{\Gamma_{-0}}\delta\chi^-(M^-\mu^{-^*} - \eta^*)\cdot\mathbf{N}\,\mathrm{d}S = 0 \tag{51}$$

Since $\delta\chi^s$, $\delta\chi^w$, $\delta\chi^+$, $\delta\chi^-$, $\delta\chi^p$ and $\delta\chi^\eta$ are arbitrary functions, the following relationships can be obtained from Equation (51):

$$\int_{\Omega_0}(\mathbf{S}^E - pJ\mathbf{C}^{-1}) : \nabla_0 \otimes \delta\chi^s\,\mathrm{d}V = \int_{\Gamma_0}\delta\chi^s\cdot\mathbf{t}^*\,\mathrm{d}S \tag{52}$$

$$\int_{\Omega_0}\left((p-\pi)\nabla_0\cdot\delta\chi^{\mathrm{w}}-\delta\chi^{\mathrm{w}}\left[\mathbf{K}^{-1}\cdot\mathbf{W}-\frac{RT}{\phi^{\mathrm{w}}}\mathbf{D}^{+^{-1}}\cdot(\mathbf{J}^{+}-c^{+}\mathbf{W})-\frac{RT}{\phi^{\mathrm{w}}}\mathbf{D}^{-^{-1}}\cdot(\mathbf{J}^{-}-c^{-}\mathbf{W})\right]\right)\mathrm{d}V$$

$$=\int_{\Gamma_{\mathrm{w}0}}\delta\chi^{\mathrm{w}}(p^{*}-\pi^{*})\cdot\mathbf{N}\,\mathrm{d}S \tag{53}$$

$$\int_{\Omega_0}\left((M^{+}\mu^{+}+\eta)\nabla_0\cdot\delta\chi^{+}-\delta\chi^{+}\left[\frac{RT}{\tilde{c}^{+}}\mathbf{D}^{+^{-1}}\cdot(\mathbf{J}^{+}-c^{+}\mathbf{W})\right]\right)\mathrm{d}V$$

$$=\int_{\Gamma_{+0}}\delta\chi^{+}(M^{+}\mu^{+^{*}}+\eta^{*})\cdot\mathbf{N}\,\mathrm{d}S \tag{54}$$

$$\int_{\Omega_0}\left((M^{-}\mu^{-}-\eta)\nabla_0\cdot\delta\chi^{-}-\delta\chi^{-}\left[\frac{RT}{\tilde{c}^{-}}\mathbf{D}^{-^{-1}}\cdot(\mathbf{J}^{-}-c^{-}\mathbf{W})\right]\right)\mathrm{d}V$$

$$=\int_{\Gamma_{-0}}\delta\chi^{-}(M^{-}\mu^{-^{*}}-\eta^{*})\cdot\mathbf{N}\,\mathrm{d}S \tag{55}$$

$$\int_{\Omega_0}\delta\chi^{p}[J-1+\nabla_0\cdot\mathbf{Q}]\,\mathrm{d}V=0 \tag{56}$$

$$\int_{\Omega_0}\delta\chi^{\eta}[-\nabla_0\cdot\mathbf{Q}^{+}+\nabla_0\cdot\mathbf{Q}^{-}]\,\mathrm{d}V=0 \tag{57}$$

Among them, Equations (52)–(55) are equilibrium relationships between internal and external parts of the force, the chemical potential of the fluid and the ionic electrochemical potentials, respectively, whereas Equations (56) and (57) remain the incompressible and electroneutral constraint conditions.

When applying the Galerkin procedure to the spatial discretization, the same function spaces are introduced for both trial and weighting functions of the variables in an element as

$$\mathbf{u}^{\mathrm{s}}=\mathbf{N}^{\mathrm{s}}\mathbf{u}^{\mathrm{s}(n)}\quad\delta\chi^{\mathrm{s}}=\mathbf{N}^{\mathrm{s}}\delta\chi^{\mathrm{s}(n)} \tag{58}$$

$$\mathbf{Q}=\mathbf{H}\mathbf{Q}^{(f)}\quad\delta\chi^{\mathrm{w}}=\mathbf{H}\delta\chi^{\mathrm{w}(f)} \tag{59}$$

$$\mathbf{Q}^{+}=\mathbf{H}^{+}\mathbf{Q}^{+(g)}\quad\delta\chi^{+}=\mathbf{H}^{+}\delta\chi^{+(g)} \tag{60}$$

$$\mathbf{Q}^{-}=\mathbf{H}^{-}\mathbf{Q}^{-(h)}\quad\delta\chi^{-}=\mathbf{H}^{-}\delta\chi^{-(h)} \tag{61}$$

$$p=\mathbf{M}p^{(m)}\quad\delta\chi^{p}=\mathbf{M}\delta\chi^{p(m)} \tag{62}$$

$$\eta=\mathbf{M}^{\eta}\eta^{(k)}\quad\delta\chi^{\eta}=\mathbf{M}^{\eta}\delta\chi^{\eta(k)} \tag{63}$$

where the superscripts (n), (f), (g), (h), (m) and (k) indicate nodal values and $\mathbf{N}$, $\mathbf{H}$, $\mathbf{H}^{+}$, $\mathbf{H}^{-}$, $\mathbf{M}$ and $\mathbf{M}^{\eta}$ are shape function matrices of the variables, respectively. By substituting Equations (58)–(63) into Equations (52) to (57), the discretized differential equations including

time derivatives of the variables are obtained. These equations are usually non-linear and have to be solved via an iterative procedure (e.g. Newton–Raphson method). Appropriate linearization produces the following matrix equation for iteration (i):

$$\begin{bmatrix} \mathbf{0} & \mathbf{0} & \mathbf{0} & \mathbf{0} & \mathbf{0} & \mathbf{0} \\ \mathbf{0} & \mathbf{B_{WW}} & \mathbf{B_{WJ^+}} & \mathbf{B_{WJ^-}} & \mathbf{0} & \mathbf{0} \\ \mathbf{0} & \mathbf{B_{J^+W}} & \mathbf{B_{J^+J^+}} & \mathbf{0} & \mathbf{0} & \mathbf{0} \\ \mathbf{0} & \mathbf{B_{J^-W}} & \mathbf{0} & \mathbf{B_{J^-J^-}} & \mathbf{0} & \mathbf{0} \\ \mathbf{0} & \mathbf{0} & \mathbf{0} & \mathbf{0} & \mathbf{0} & \mathbf{0} \\ \mathbf{0} & \mathbf{0} & \mathbf{0} & \mathbf{0} & \mathbf{0} & \mathbf{0} \end{bmatrix}^{(i)} \begin{bmatrix} \Delta v^{s(n)} \\ \Delta W^{(f)} \\ \Delta J^{+(g)} \\ \Delta J^{-(h)} \\ \Delta \dot{p}^{(m)} \\ \Delta \dot{\eta}^{(k)} \end{bmatrix}^{(i)}$$

$$+ \begin{bmatrix} \mathbf{P_{uu}} & \mathbf{0} & \mathbf{0} & \mathbf{0} & \mathbf{P_{up}} & \mathbf{0} \\ \mathbf{P_{Qu}} & \mathbf{0} & \mathbf{P_{QQ^+}} & \mathbf{P_{QQ^-}} & \mathbf{P_{Qp}} & \mathbf{0} \\ \mathbf{P_{Q^+u}} & \mathbf{0} & \mathbf{P_{Q^+Q^+}} & \mathbf{0} & \mathbf{0} & \mathbf{P_{Q^+\eta}} \\ \mathbf{P_{Q^-u}} & \mathbf{0} & \mathbf{0} & \mathbf{P_{Q^-Q^-}} & \mathbf{0} & \mathbf{P_{Q^-\eta}} \\ \mathbf{P_{pu}} & \mathbf{P_{pQ}} & \mathbf{0} & \mathbf{0} & \mathbf{0} & \mathbf{0} \\ \mathbf{0} & \mathbf{0} & \mathbf{P_{\eta Q^+}} & \mathbf{P_{\eta Q^-}} & \mathbf{0} & \mathbf{0} \end{bmatrix}^{(i)} \begin{bmatrix} \Delta u^{s(n)} \\ \Delta Q^{(f)} \\ \Delta Q^{+(g)} \\ \Delta Q^{-(h)} \\ \Delta p^{(m)} \\ \Delta \eta^{(k)} \end{bmatrix}^{(i)} = \begin{bmatrix} \mathbf{G_{ext}} - \mathbf{G_{int}^{(i-1)}} \\ \mathbf{\Xi_{ext}^{w}} - \mathbf{\Xi_{int}^{w(i-1)}} \\ \mathbf{\Xi_{ext}^{+}} - \mathbf{\Xi_{int}^{+(i-1)}} \\ \mathbf{\Xi_{ext}^{-}} - \mathbf{\Xi_{int}^{-(i-1)}} \\ -\mathbf{\Lambda}^{(i-1)} \\ -\mathbf{\Phi}^{(i-1)} \end{bmatrix} \tag{64}$$

where $\mathbf{G_{int}}$ is the equivalent internal nodal force of the tissue and $\mathbf{\Xi_{int}^{w}}$, $\mathbf{\Xi_{int}^{+}}$ and $\mathbf{\Xi_{int}^{-}}$ are equivalent internal nodal chemical potentials of the fluid and the electrochemical potentials of the ions, respectively. Correspondingly, the equivalent external nodal force, nodal chemical potential of the fluid and the electrochemical potentials of the ions are defined sequentially as $\mathbf{G_{ext}}$, $\mathbf{\Xi_{ext}^{w}}$, $\mathbf{\Xi_{ext}^{+}}$ and $\mathbf{\Xi_{ext}^{-}}$. $\mathbf{\Lambda}$ and $\mathbf{\Phi}$ are vectors standing for the residuals of the incompressible and electroneutral constraints at the nodes, respectively. Differential equation (64) with respect to time is solved by applying backward Eular temporal discretization. The details of the element matrix and vectors are shown in the Appendix.

4. NUMERICAL EXAMPLES

4.1. Stress relaxation in confined compression problem

In confined compression, the soft tissue is placed in an open rigid chamber with an impermeable wall and bottom. The deformation is caused axially by the movement of a rigid porous platen on the top (Figure 2(a)). Due to the complexity of the triphasic theory, the analytical solution does not exist even for such a virtually one-dimensional problem. Mow *et al.* [24] solved stress relaxation in a confined compression problem by applying the finite difference method (FDM) to the triphasic theory under the assumption of small deformation. The linear approximations

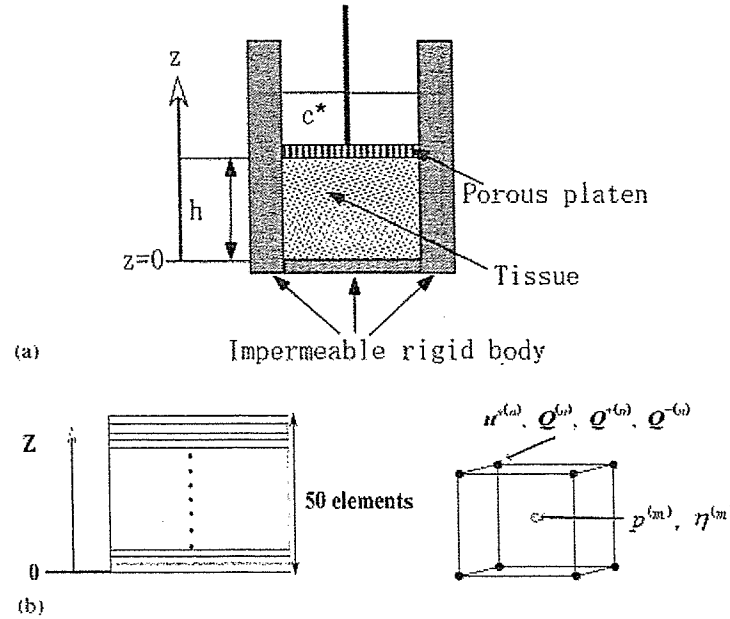

Figure 2. Demonstration of the confined compression configuration and the finite element model: (a) confined compression configuration; and (b) finite element model and the nodal variables.

of deformation-dependent porosity and FCD were introduced in FDM as

$$\phi^{\mathrm{w}} = \phi_0^{\mathrm{w}} + e_z(1 - \phi_0^{\mathrm{w}}) \tag{65}$$

$$c^{\mathrm{F}} = c_0^{\mathrm{F}}(1 - e_z/\phi_0^{\mathrm{w}}) \tag{66}$$

where e_z is the strain in the axial direction and ϕ_0^{w} and c_0^{F} are the porosity and FCD per unit volume of interstitial water before deformation, respectively.

To verify the implementation of the proposed procedure, a confined problem is analysed and the results are compared with those obtained by the FDM of Mow *et al.* [24]. The assumption of small deformation and linear approximations (65) and (66) are adopted for the comparability. The dimensions of the cartilage specimen are set to be $1.0 \times 1.0 \times 0.5$ mm. Assuming that the tissue is an isotropic material, the material parameters are selected to be the same as those in Reference [24]: $c_0^{\mathrm{F}} = 0.2$ Eq/l, $\phi_0^{\mathrm{s}} = 0.25$, $d^{+} = 0.5 \times 10^{-9}\,\mathrm{m}^2/\mathrm{s}$, $d^{-} = 0.8 \times 10^{-9}\,\mathrm{m}^2/\mathrm{s}$, $\kappa = (\phi^{\mathrm{w}}/7.0 \times 10^{14})\,\mathrm{m}^4/\mathrm{N\,s}$ and $\gamma^{\pm} = \gamma^{\pm *} = \Phi = 1.0$. The aggregate modulus of the tissue defined as $H_{\mathrm{A}} = \lambda_{\mathrm{s}} + 2\mu_{\mathrm{s}}$ is 0.3 MPa with λ_{s} and μ_{s} being Lamé coefficients of the solid matrix. The external bath concentration c^* is 0.15 M NaCl at a temperature $T = 298$ K, while the universal gas constant R is 8.314 J/mol K. A ramp compression displacement is applied on the top of the cartilage which has been equilibrated in external NaCl solution bath for 200 s with a uniform velocity of 0.25 μm/s to get a 10% surface-to-surface strain. Beyond 200 s, the platen is kept in a fixed position, until the specimen undergoes stress relaxation to the final equilibrium state [24].

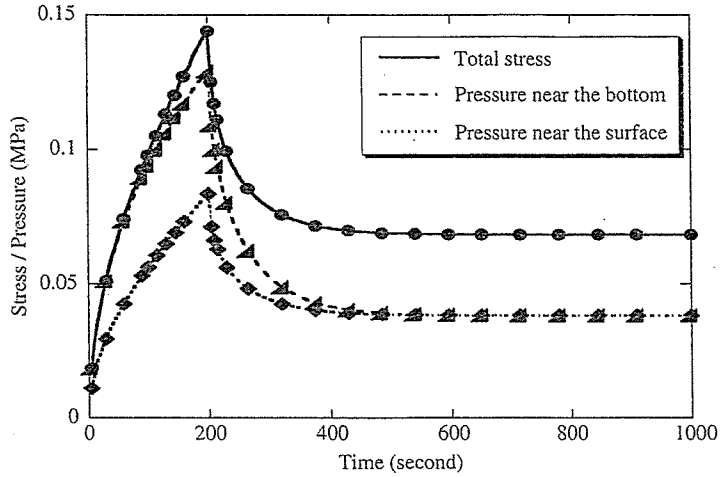

Figure 3. Comparison of total stress and fluid pressure histories obtained by FDM (lines) and FEA (symbols).

The finite element model is constructed with fifty equally divided hexahedral elements in the thickness shown in Figure 2(b). The Q1/Q0 elements, i.e. trilinear interpolation for solid displacement, fluid flow, and ionic molar flows while uniform for hydrostatic pressure and electrical potential, are adopted. Figure 3 shows that the total stresses, which are obtained from the load divided by the area of the fluid pressure obtained by FEA are in good agreement with those obtained by FDM.

Next, the effects of the linear approximations of porosity and the FCD (Equations (65) and (66)) on the behaviours of the tissue during confined compression are investigated. The same material model is applied while the accurate forms of porosity and FCD are introduced as follows. With the assumption that ionic volumes can be neglected, consideration of the saturated condition $\phi^{\mathrm{w}} = 1 - \phi^{\mathrm{s}}$ and $\phi_0^{\mathrm{s}} = J\phi^{\mathrm{s}}$ leads to

$$\phi^{\mathrm{w}} = 1 - \frac{\phi_0^{\mathrm{s}}}{J} \tag{67}$$

where ϕ_0^{s} is the initial solidity, while the electroneutral constraint gives

$$c^{\mathrm{F}} = c^{+} - c^{-} \tag{68}$$

Figure 4 shows the total stresses and the hydrostatic pressures near the loaded surface with the maximum strain value of 18.5% obtained by linear and non-linear analyses. It can be seen from Figure 4 that the linear analysis predicts a smaller total stress and pressure near the upper surface. The relative deviations of hydrostatic pressure between the results of the non-linear and linear analyses are about 8.7% at the end of loading and 13.7% in the equilibrium state. For the total stress, since the deformation occurred mainly near the upper surface during the loading process, the relative deviations between linear and non-linear analyses are relatively small (3.0% at the end of loading), whereas, the effects of non-linearity raised the relative deviation of the total stress to about 10.3% in the equilibrium state due to the deformation that occurred in

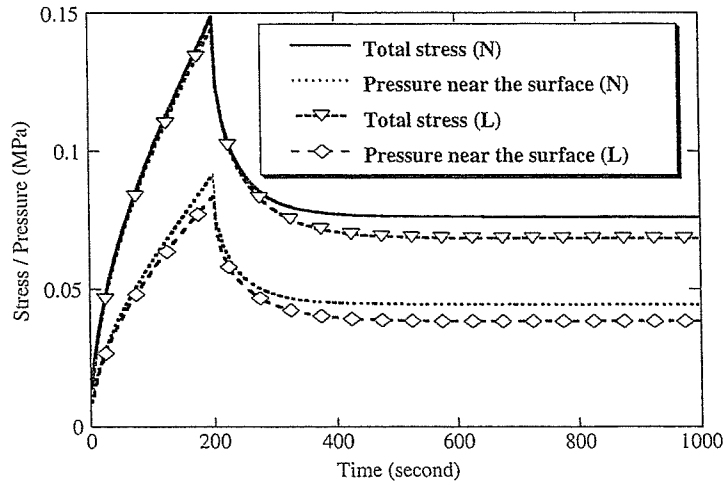

Figure 4. Comparison of results of the linear and non-linear analyses for the confined compression problem (L: linear analysis; N: non-linear analysis).

the whole tissue. These observations show that, even in problems with relatively small global deformation, the effects of non-linear porosity and FCD due to local large deformation on the mechanical behaviours of the tissue, cannot be neglected.

4.2. Three-dimensional simulation of articular cartilage curling phenomena

The existence of FCD causes different ionic concentrations, and thus different osmotic pressures inside and outside the tissue. Such differences of osmotic pressure are well known as the Donnan osmotic pressure which increases with FCD. Investigators [25] found that the Donnan osmotic pressure contributes over 85% of the total measured swelling pressure, while the rest is caused by other effects such as charge–charge repulsion. Since in this research, only ionic effects on swelling are considered, Donnan osmotic pressure is used to represent the swelling pressure of the tissue. The Donnan osmotic pressure behaves as a chemical load on the hydrated soft tissue [26] leading to fluid flowing and as a consequence, results in a hydrostatic pressure in the tissue. Even in the absence of a mechanical load, the resulting hydrostatic pressure is counteracted by the internal force of ECM resisting dilation and hence produces a pre-stress state in the cartilage. Since the non-uniform distribution of FCD in cartilage causes a distributed Donnan osmotic pressure, the cartilage curls up immediately when excised from the subchondral bone due to the non-uniform pre-stressed state of the solid matrix. Also, after being submerged in a solution bath, the shape and dimensions of the cartilage change according to the concentration of the solution. In this section, the curling phenomena of articular cartilage in solutions with various concentrations are simulated by taking into account the geometric and material non-linearities due to large deformation, and moreover, non-uniform distributions of solidity and FCD. The results are compared with those obtained by experiment to verify the effectiveness of the proposed procedure.

In experiments [19], the strips were submerged in NaCl solutions with concentrations of 2, 0.5, 0.15, 0.05 and 0.015 M to equilibrate. The state of the tissue in 2 M NaCl was used

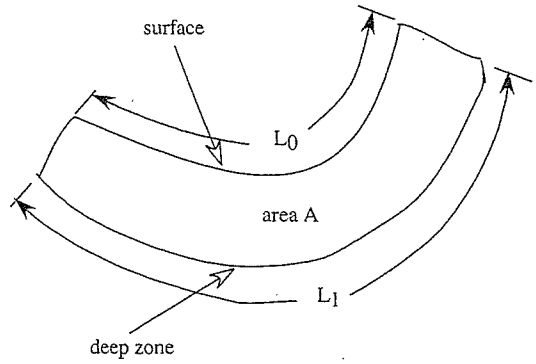

Figure 5. Schematic definition for lengths of sample edges and cross-section area.

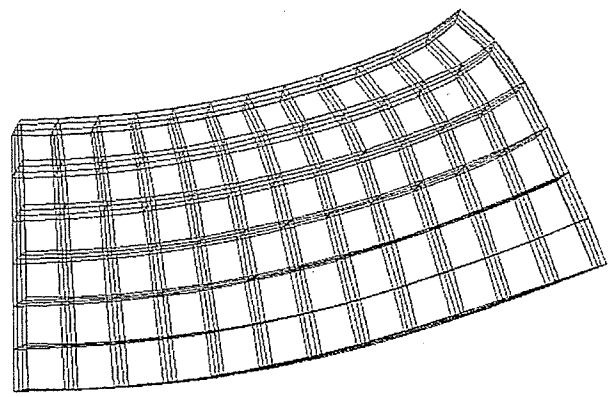

Figure 6. Finite element model of the $\frac{1}{4}$ cartilage strip.

as a hypertonic reference. The lengths of sample edges L_0, L_1 and the cross-sectional area A (Figure 5) were measured. The swelling induced stretch defined as $\lambda_0 = L_0(c^*)/L_0(2M)$, $\lambda_1 = L_1(c^*)/L_1(2M)$ and areal change defined as $\Delta A/A = A(c^*)/A(2M)$ were taken as the swelling parameters, where c^* denotes the varying outside concentration. These conditions and definitions were also introduced into the numerical simulation. One fourth of the articular cartilage strips ($0.85 \times 2 \times 4$ mm in width $\times$ height $\times$ length) were modelled with 216 hexahedral Q1/Q0 elements (Figure 6) and symmetric boundary conditions were applied. The distributions of solidity and FCD measured by Maroudas *et al.* [27] and Mow *et al.* [28] (Figures 7 and 8) were used in the numerical simulation. The deformation-dependent function of the permeability proposed by Holmes *et al.* [29] as $\kappa = \kappa_0[(J-1+\phi_0^w)/\phi_0^w]\text{EXP}[\omega \times (J^2-1)]$ (with κ_0 the initial permeability and ω the material constant obtained by curve fitting) was chosen as the non-linear permeability model during the deformation. The other material parameters of the articular cartilage were selected within the ranges of published values as in References [1, 11, 16, 24] $\kappa_0 = 5 \times 10^{-16}\text{m}^4/\text{N s}$, $\omega = 1.0$, $d^+ = 0.5 \times 10^{-9}\text{m}^2/\text{s}$ and $d^- = 0.8 \times 10^{-9}\text{m}^2/\text{s}$. The Helmholtz free energy of the Mooney–Rivlin material model was employed for the solid

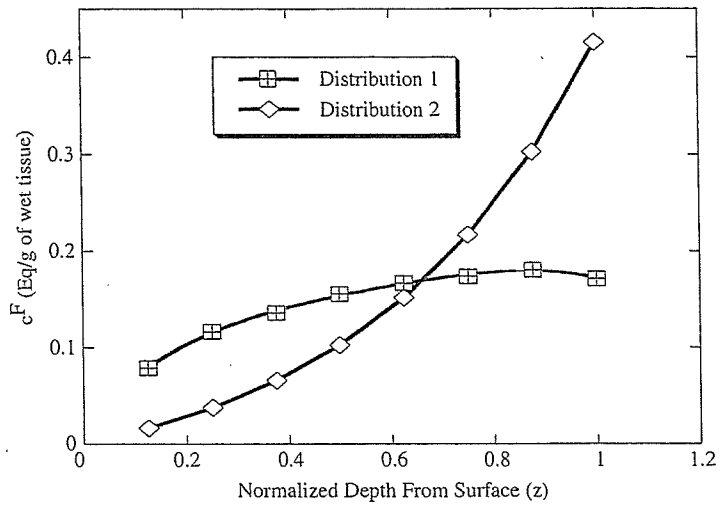

Figure 7. Distributions of FCD in depth: distribution 1 is obtained in Reference [27]; distribution 2 is assumed by maintaining the mean value the same as distribution 1.

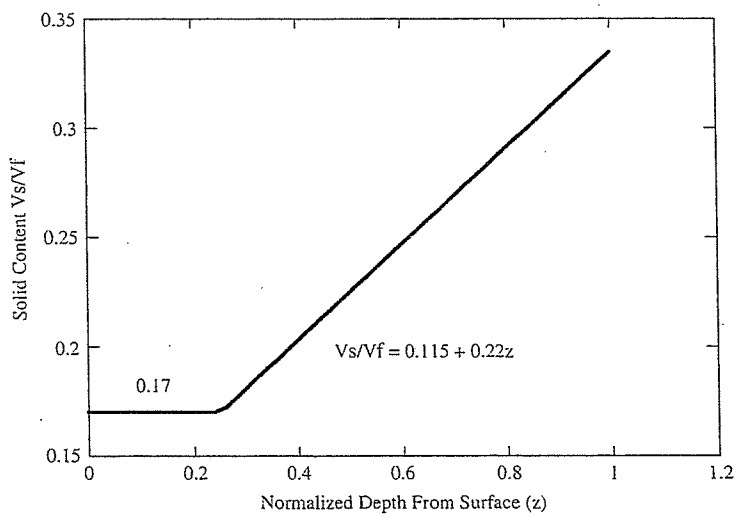

Figure 8. Distribution of solidity in depth [28].

phase in the form of $U = C_1(\tilde{I}_1 - 3) + C_2(\tilde{I}_2 - 3)$, where $\tilde{I}_1$ and $\tilde{I}_2$ are the first and second reduced invariants of the right Cauchy–Green deformation tensor and C_1 and C_2 are material constants assigned the values 0.024 and 0.072, respectively, which correspond to Young's modulus $\mathbf{E}_s = 0.5\,\text{MPa}$ and Poisson's ratio $\nu_s = 0.3$ for the solid phase in the case of infinitesimal deformation.

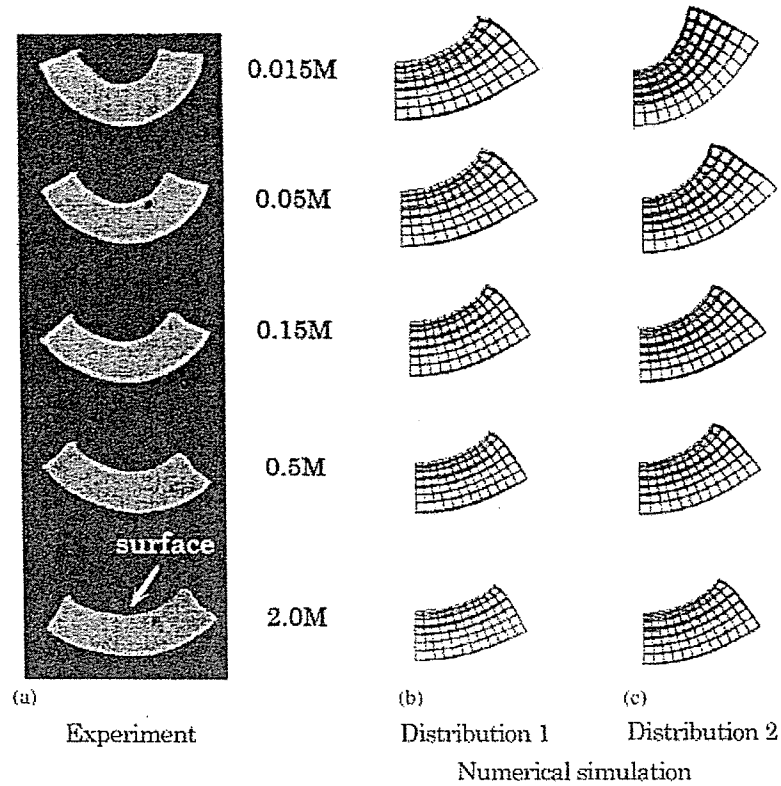

Figure 9. Curling deformation obtained by experiments and numerical simulations: (a) photos taken in experiment in Reference [19] (Reproduced by permission of Copyright © 1998 by ASME); (b) numerical results with FCD distribution 1 in Figure 7; and (c) numerical results with FCD distribution 2 in Figure 7.

As shown in Figure 9, consistent with experimental observation, the results of the numerical simulation show that the curling effect increased in the solution with lower concentration compared with the hypertonic reference state of 2 M NaCl. It should be mentioned that the results of the numerical analysis are significantly affected by the distributions of FCD, permeability, and internal structure of the articular cartilage. As an example, the results based on the FCD distribution obtained by Maroudas *et al.* [27] and another by maintaining the mean value the same as the former one, are shown for comparison in Figures 9(b) and (c). Also, to investigate the curling phenomena precisely, the anisotropic structure of the articular cartilage must, in future, be taken into account. On the other hand, the swelling parameters, λ_0, λ_1 and $\Delta A/A$ obtained by FEA increased with decrease in the solution concentration, while the experimental results (Figure 10) show the same tendencies except for λ_0 (Figure 10(a)). The decrease of parameter λ_0 in the experiments indicates shrinkage of the surface occurred in the solution with lower concentration. Setton *et al.* [19] investigated the behaviour of the layer near the cartilage surface and found that swelling there was greatly limited. In an experiment

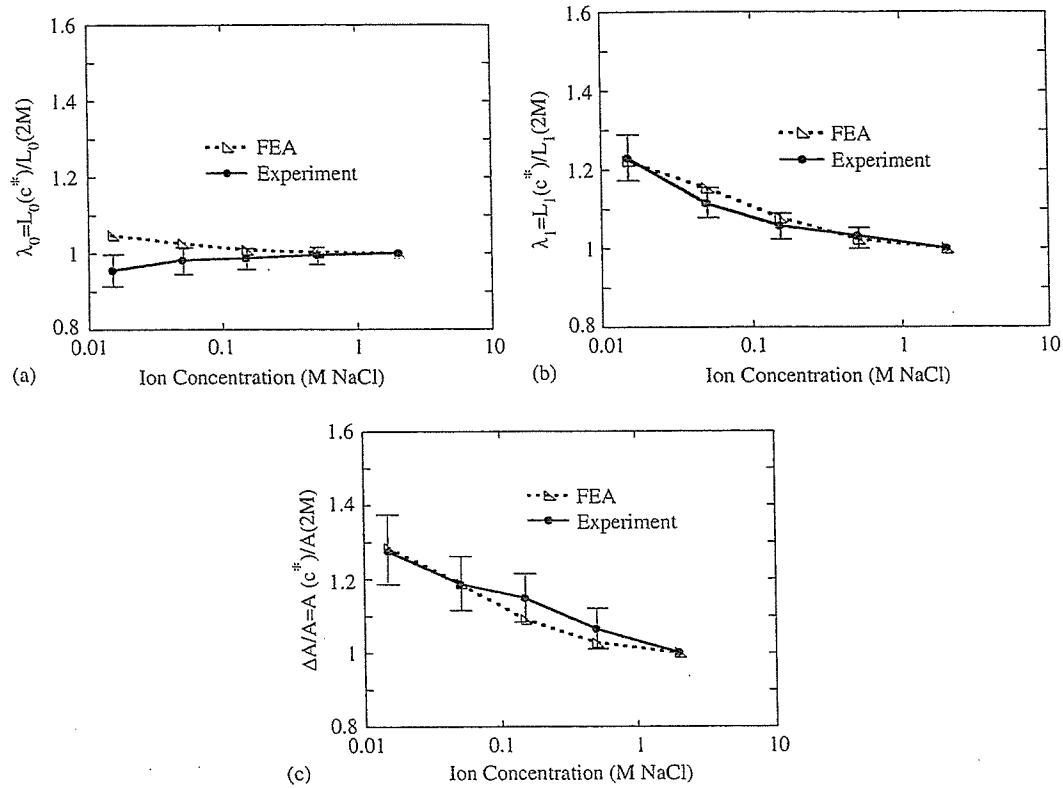

Figure 10. Experimental and FEA results corresponding to FCD distribution 1 in Figure 7 of swelling parameters vs external solution concentration.

for comparison, Setton measured the swelling parameters after removing the surface zone in a physiologic solution (0.15 M NaCl) and found that λ_0 also increased to 1.049 ± 0.034 [19]. The numerical result $\lambda_0 = 1.009$ comparable with this experimental result is considered to be attributable to the neglect of the special structure of the cartilage surface.

Variations with time of the hydrostatic pressure and Donnan osmotic pressure distributions in the depth direction at the transverse mid-plane of the cartilage strip, are shown in Figure 11. Once the cartilage strip was immersed in the solution, the Donnan osmotic pressure induced fluid flow into the cartilage and increased the hydrostatic pressure in the tissue. The hydrostatic pressure was highest in the deep zone and increased with time as shown in Figure 11(a). Since there is no mechanical load on the cartilage strip, the distributed hydrostatic pressure due to the distributed FCD, produced differential swelling which led to curling of the cartilage strip. Figure 11(a) indicates that the cartilage swelled quickly, particularly in the deep zone, within 100 s after being submerged in the solution. By 1000 s, the tissue almost reached equilibrium with the largest hydrostatic pressure near the deep zone indicating maximum swelling of the solid matrix. It is noted that the hydrostatic pressure near the surface at 100 s with a negative value implies a sudden tension state of ECM, which may be due to the sudden significant swelling near the deep zone. Figure 11(b) shows that the distribution of the Donnan osmotic

